KJOAS

ISSN (Print) : 2466-2402
ISSN (Online) : 2466-2410

REVIEW ARTICLE

Survey of spatial and temporal landslide prediction methods and techniques

Hyunuk An[1], Minseok Kim[2], Giha Lee[3]*, Tran The Viet[3]

[1]Department of Agricultural & Rural Engineering Chungnam National University, Daejeon 34134, Korea
[2]International Water Resources Research Institute, Chungnam National University, Daejeon 34134, Korea
[3]Department of Construction & Disaster Prevention Engineering Kyungpook National University, Sangju 37224, Korea

*Corresponding author: leegiha@knu.ac.kr

Abstract

Landslides are one of the most common natural hazards causing significant damage and casualties every year. In Korea, the increasing trend in landslide occurrence in recent decades, caused by climate change, has set off an alarm for researchers to find more reliable methods for landslide prediction. Therefore, an accurate landslide-susceptibility assessment is fundamental for preventing landslides and minimizing damages. However, analyzing the stability of a natural slope is not an easy task because it depends on numerous factors such as those related to vegetation, soil properties, soil moisture distribution, the amount and duration of rainfall, earthquakes, etc. A variety of different methods and techniques for evaluating landslide susceptibility have been proposed, but up to now no specific method or technique has been accepted as the standard method because it is very difficult to assess different methods with entirely different intrinsic and extrinsic data. Landslide prediction methods can fall into three categories: empirical, statistical, and physical approaches. This paper reviews previous research and surveys three groups of landslide prediction methods.

Keywords: factor of safety, landslide prediction, landslide warning system, landslide, rainfall threshold

Citation: An HU, Kim MS, Lee GH, Viet TT. 2016. Survey of spatial and temporal landslide prediction methods and techniques. Korean Journal of Agricultural Science 43:507-521.

DOI: http://dx.doi.org/10.7744/kjoas.20160053

Editor: Sun-Ok Chung, Chungnam National University, Korea

Received: December 13, 2016

Revised: December 28, 2016

Accepted: December 29, 2016

Introduction

Landslides are one of the most common natural hazards causing significant damage and casualties every year. Landslides often occur in the soil mantle due to extreme rainfall and can present hazards to human life, property, and activities. They can also trigger rapidly moving debris flows (Iverson, 1997). The Republic of Korea also frequently suffers from landslides and slope instabilities with mountainous regions covering more than 70% of the land area. Statistics provided by the Korea Forest Service in 2013 showed that landslides in Korea are becoming more frequent and severe in recent years. The 10-year average for recorded landslide-damaged areas increased from 321 ha in the 1980s to 349 ha in the 1990s and 713 ha in the 2000s; this is more than double the values of previous decades. Since the year 2000, in particular, more than 1,000 ha of landslide-damaged

areas have been recorded (Kim et al., 2014). Additionally, landslides are responsible for the loss of approximately 23 lives each year, which comprises approximately 25% of the annual casualties as a result of a natural disaster in Korea (Lee and Park, 2014).

An accurate landslide-susceptibility assessment is fundamental for preventing landslides and minimizing damages. Especially, the increasing trend in landslide occurrence in mountainous areas in recent decades caused by climate change has set off an alarm for researchers to seek more reliable methods for landslide prediction and warning systems. However, analyzing the stability of a natural slope is not an easy task because it depends on numerous factors such as those related to vegetation, soil properties, soil moisture distribution, the amount and duration of rainfall, earthquake, etc. The factors causing landslide hazards can be categorized into two groups: intrinsic variables, such as geological conditions or vegetation, and extrinsic variables such as rainfall, earthquake, or human activity. The probability of landslide occurrence depends on both of the above variables. The spatial distribution of the intrinsic variables determine the spatial distribution of landslide susceptibility in the study region (Huabin et al., 2005); and the time of occurrence of extrinsic variables is important for estimating the time of landslide occurrence.

A variety of different methods and techniques for evaluating landslide susceptibility have been proposed, but up to now, no specific method or technique has been accepted as the standard approach because it is very difficult to assess the different methods with entirely different intrinsic and extrinsic data. There is hardly any systematic comparison of different methods, in terms of respective advantages and limitations (Carrara et al., 1995; Westen et al., 1997; Huabin et al., 2005). Landslide prediction methods can fall into three categories: empirical, statistical, and physical approaches. This paper reviews previous research and surveys three groups of landslide prediction methods.

Empirical approaches

One of the most common approaches for the prediction of landslide occurrence is the estimation of rainfall threshold, which is derived from two or more rainfall parameters such as rainfall intensity and duration. Since the pioneering works of Caine (1980), Campbell (1975), Guidicini and Iwasa (1977), and Lumb (1975), the rainfall threshold approach has been widely used and many thresholds levels for rainfall-induced shallow landslides have been proposed based on a large variety of rainfall parameters. Huang et al. (2015) classify those methods according to the type of data the threshold is based on, such as (i) hourly rainfall intensity and duration (Keefer et al., 1987; Guzzetti et al., 2007b; Cannon et al., 2008; Segoni et al., 2014), which is the most popular among rainfall threshold methods; (ii) daily rainfall and antecedent rainfall intensity (Glade et al., 2000; Guo et al., 2013); (iii) cumulative rainfall and duration (Aleotti, 2004); (iv) cumulative rainfall and average rainfall intensity (Hong et al., 2005); and, (v) a combination of different thresholds such as (i) - (iv) (Baum and Godt, 2009). The rainfall threshold method is useful for early warning systems due to its simplicity and applicability. The performance of the rainfall threshold method has been proven in many studies (Keefer et al., 1987; Baum and Godt, 2009; Glade et al., 2000; Guzzetti et al., 2007a; Osanai et al., 2010; Greco et al., 2013; Segoni et al., 2014; Zêzere et al., 2014; Segoni et al., 2015).

The empirical rainfall threshold can be simply estimated by drawing lower-bound lines to the rainfall conditions that resulted in landslides plotted in Cartesian, semi-logarithmic, or logarithmic coordinates without any rigorous mathematical, statistical, or physical criterion. Guzzetti et al. (2007b) listed 25 rainfall and climate variables used in previous studies of empirical rainfall thresholds for shallow landslide as listed in Table 1.

Table 1. Rainfall and climate variables for the definition of rainfall thresholds for shallow landslides listed in Guzzetti et al. (2007b). Table lists the variables, the units of measure most commonly used for the parameter.

Variables	Description	Units
D	Rainfall duration. The duration of the rainfall event or rainfall period.	hr or day
D_c	Duration of the critical rainfall event.	hr
$E_{(h),(d)}$	Cumulative event rainfall. The total rainfall measured from the beginning of the rainfall event to the time of failure. Also known as storm rainfall. “h” indicates the considered period in hours; “d” indicates the considered period in days.	Mm
E_{Map}	Normalized cumulative event rainfall. Cumulative event rainfall divided by Map. Also known as normalized storm rainfall.	-
C	Critical rainfall. The total amount of rainfall from the time of a distinct increase in rainfall intensity (t_0) to the time of the triggering of the first landslide (t_f).	Mm
C_{Map}	Normalized critical rainfall. Critical rainfall divided by MAP.	-
R	Daily rainfall. The total amount of rainfall for the day of the landslide event.	Mm
R_{Map}	Normalized daily rainfall. Daily rainfall divided by MAP.	mm
I	Rainfall intensity. The amount of precipitation in a period, i.e., the rate of precipitation over the considered period. Depending on the duration of the measuring period, rainfall intensity measures peak or average precipitation rates.	mm/h
I_{Map}	Normalized rainfall intensity. Rainfall intensity divided by MAP	1/h
I_{max}	Maximum hourly rainfall intensity. The maximum hourly rainfall intensity.	mm/h
I_p	Peak rainfall intensity. The highest rainfall intensity (rainfall rate) during a rainfall event. Available from detailed rainfall records.	mm/h
	Mean rainfall intensity for final storm period. “h” indicates the considered period, in hours, most commonly from 3 to 24 hours.	mm/h
I_c	Critical hourly rainfall intensity.	mm/h
I_f	Rainfall intensity at the time of the slope failure. Available from detailed rainfall records.	mm/h
I_{fMap}	Normalized rainfall intensity at the time of the slope failure. Rainfall intensity at the time of the slope failure divided by MAP	1/h
$A_{(d)}$	Antecedent rainfall. The total (cumulative) precipitation measured before the landslide triggering rainfall event. “d” indicates the considered period in days.	Mm
A_{Map}	Normalized antecedent rainfall. Antecedent rainfall divided by MAP	-
$A_{(y)}$	Antecedent yearly precipitation up to date of the event. The total (cumulative) yearly precipitation measured before the landslide triggering rainfall event.	Mm
$A_{(y)Map}$	Normalized antecedent yearly precipitation up to date of the event. Antecedent yearly precipitation divided by MAP.	-
Fc	Sum of normalized antecedent yearly precipitation and normalized event rainfall. Also known as “final coefficient”.	-
Map	Mean annual precipitation. For a rain gauge, the long term yearly average precipitation, obtained from historical rainfall records. A proxy for local climatic conditions.	Mm
RDs	Average number of rainy-days in a year. For a rain gauge, the long term yearly average of rainy (or wet) days, obtained from historical rainfall records. A proxy for local climatic conditions.	#
RDN	Rainy-day normal. For a rain gauge, the ratio between the MAP and the average number of rainy-days in a year.	mm/#
N	Ratio between the MAP of two different (distant) areas.	-

The threshold based on hourly rainfall intensity and duration has a general form as follows:

$$I = c + aD^b \quad (1)$$

where I is mean rainfall intensity, D is rainfall duration, and a, b, and c are parameters. Note that if c = 0, Eq. (1) is a simple power law. The above equation covers a wide range of rainfall duration between 1 and 100 hr and intensities between 1 and 200 mm/hr. Guzzetti et al. (2007b) listed 52 rainfall intensity-duration thresholds from previous studies. Among them, 45 thresholds use a simple power law (c = 0). The range of parameter a is from 4.0 to 176.4 and b is from -1.5 to -0.19. As stated above, this method can straightforwardly be applied to a wide range of rainfall intensities and durations. However, its limitation is that a very small rainfall intensity with very long duration may result in landslides, which is unrealistic. In order to overcome this limitation, some studies proposed the minimum value of rainfall intensity for long rainfall durations in the range from 0.48 to 6.90 mm/hr. By analyzing variety of rainfall intensity-duration thresholds as listed in Table 2, Guzzetti et al. (2007b) found that those local thresholds are slightly higher than the regional thresholds and that global thresholds are positioned in a lower part than the regional and local thresholds. They also found that there are significant differences in thresholds even for the same geographical areas. The reason for this is that landslides do not only depend on the rainfall conditions but also physiographical, geological, or geomorphological conditions.

A few studies proposed probabilistic rainfall thresholds (e.g., Berti et al., 2012; Huang et al., 2015). A rainfall threshold is defined as the value that must be exceeded to result in landslides. This definition is based on a deterministic view: the system of the landslide can be predicted by comparing the input value (rainfall) with the threshold, and no randomness is involved in the system. Such a deterministic approach can be successfully used to define the rainfall threshold in the ideal cases, where a triggering mechanism is directly controlled by rainfall (Berti et al., 2012). In most of the real cases, however, the separation between critical and non-critical rainfall is not clear. Fig. 1 shows a conceptual example to demonstrate the difficulty of determining rainfall threshold. Since the landslide events are triggered by the combination of various factors, the occurrence of the landslide cannot be predicted by rainfall alone. Therefore, the deterministic approach has limitations, and a probabilistic model is required for more accurate prediction. Berti et al. (2012) proposed the probabilistic rainfall thresholds using a Bayesian approach as follows:

$$P(A|B) = \frac{P(B|A) \cdot P(A)}{P(B)} \quad (2)$$

where $P(A|B)$ is the conditional probability of observing a landslide when a rainfall event of magnitude B occurs, $P(A)$ is the prior probability of landslide occurrence regardless of whether a rainfall event of magnitude B occurs or not, $P(B)$ is the marginal probability of observing a rainfall of magnitude B irrespective of whether a landslide occurs or not, and $P(B|A)$ is the conditional probability of observing a rainfall event of magnitude B when a landslide occurs. Huang et al. (2015) proposed the probability of landslide occurrence (PLO) as follows:

$$PLO = \sqrt{\frac{C - C_{\min}}{C_{\max} - C_{\min}}} \quad (3)$$

$$C = R + aI \quad (4)$$

Table 2. Rainfall intensity duration thresholds for the initiation of landslides listed in Guzzetti et al. (2007a).

Extent[z]	Area	L. Type	Equation	Range
G	World	ShD	I = 14.82 × D-0.39	0.167 < D < 500
R	Carinthia and E Tyrol Austria	S	I = 41.66 × D-0.77	1 < D < 1,000
L	Valtellina Lombardy N Italy	S	I = 44.668 × D-0.78	1 < D < 1,000
L	San Francisco Bay Region California	D	I = 6.9+38 × D-1.00	2 < D < 24
L	San Francisco Bay Region California	D	I = 2.5+300 × D-2.0	5.5 < D < 24
L	Central Santa Cruz Mountains California	D	I = 1.7+9 × D-1.00	1 < D < 6.5
R	Indonesia	D	I = 92.06-10.68 × D1.0	2 < D < 4
R	Puerto Rico	D	I = 66.18 × D-0.52	0.5 < D < 12
R	Brazil	D	I = 63.38-22.19 × D1.0	0.5 < D < 2
R	China	D	I = 49.11-6.81 × D1.0	1 < D < 5
L	Hong Kong	D	I = 41.83 × D-0.58	1 < D < 12
R	Japan	D	I = 39.71 × D-0.62	0.5 < D < 12
R	California	D	I = 35.23 × D-0.54	3 < D < 12
R	California	D	I = 26.51 × D-0.19	0.5 < D < 12
G	World	D	I = 30.53 × D-0.57	0.5 < D < 12
R	Peri-Vesuvian area Campania Region S Italy	D	I = 176.40 × D-0.90	0.1 < D < 1,000
L	Mayon Philippine	L	I = 27.3 × D - 0.38	0.167 < D < 3
R	Lombardy N Italy	A	I = 20.1 × D - 0.55	1 < D < 1,000
R	Puerto Rico	A	I = 91.46 × D - 0.82	2 < D < 312
L	Pasig-Potrero River Philippine	L	I = 9.23 × D - 0.37	0.08 < D < 7.92
G	World	S	I = 10 × D - 0.77	0.1 < D < 1,000
L	Sacobia River Philippine	L	I = 5.94 × D - 1.50	0.167 < D < 3
R	Switzerland	A	I = 32 × D - 0.70	1 < D < 45
R	NE Alps Italy	D	I = 47.742 × D - 0.507	0.1 < D < 24
L	Rho Basin Susa Valley Piedmont NW Italy	D	I = 9.521 × D - 0.4955	1 < D < 24
L	Rho Basin Susa Valley Piedmont NW Italy	D	I=11.698 × D - 0.4783	1 < D < 24
L	Perilleux Basin Piedmont NW Italy	D	I = 11.00 × D - 0.4459	1 < D < 24
L	Perilleux Basin Piedmont NW Italy	D	I = 10.67 × D - 0.5043	1 < D < 24
L	Champeyron Basin Piedmont NW Italy	D	I = 12.649 × D - 0.5324	1 < D < 24
L	Champeyron Basin Piedmont NW Italy	D	I = 18.675 × D - 0.565	1 < D < 24
R	Campania S Italy	A	I = 28.10 × D - 0.74	1 < D < 600
L	Mettman Ridge Oregon	A	I = 9.9 × D - 0.52	1 < D < 170
L	Blue Ridge Madison County Virginia	D	I = 116.48 × D - 0.63	2 < D < 16
G	World	Sh	I=0.48 + 7.2 × D - 1.00	0.1 < D < 1,000
L	Moscardo Torrent NE Italy	A	I = 15 × D - 0.70	1 < D < 30
R	Eastern Jamaica	Sh	I = 11.5 × D - 0.26	1 < D < 150
R	North Shore Mountains Vancouver Canada	Sh	I = 4.0 × D - 0.45	0.1 < D < 150
R	Piedmont NW Italy	Sh	I = 19 × D - 0.50	4 < D < 150
L	Piedmont NW Italy	A	I = 44.668 × D - 0.78 × N	1 < D < 1,000
L	Valzangona N Apennines Italy	A	I = 18.83 × D - 0.59	24 < D < 3,360
L	Seattle Area Washington	S	I = 82.73 × D - 1.13	20 < D < 55
G	World	D	I = 7.00 × D - 0.60	0.1 < D < 3
R	Taiwan	A	I = 115.47 × D - 0.80	1 < D < 400
R	Pyrenees Spain	A	I = 17.96 × D - 0.59	D > 168
L	Apuane Alps Tuscany Italy	Sh	I = 26.871 × D - 0.638	0.1 < D < 35
L	Apuane Alps Tuscany Italy	Sh	I = 85.584 × D - 0.781	0.1 < D < 35
L	Apuane Alps Tuscany Italy	Sh	I = 38.363 × D - 0.743	0.1 < D ≤ 12
L	Apuane Alps Tuscany Italy	Sh	I = 76.199 × D - 0.692	0.1 < D ≤ 12
R	Shikoku Island Japan	A	I = 1.35+55 × D - 1.0	24 < D < 300
R	Central Taiwan	D	I = 13.5 × D - 0.20	0.7 < D < 40
R	Central Taiwan	D	I = 6.7 × D - 0.20	0.7 < D < 40
L	N of Lisbon Portugal	A	I = 84.3 × D - 0.57	0.1 < D < 2,000

[z]G, global threshold; R, regional threshold; L, local threshold. Area, the area where the threshold was defined. L. Type: A, all types; D, debris flow; S, soil slip; Sh, shallow landslide, L, lahar. Rainfall intensity in mm/hr, rainfall duration in hours.

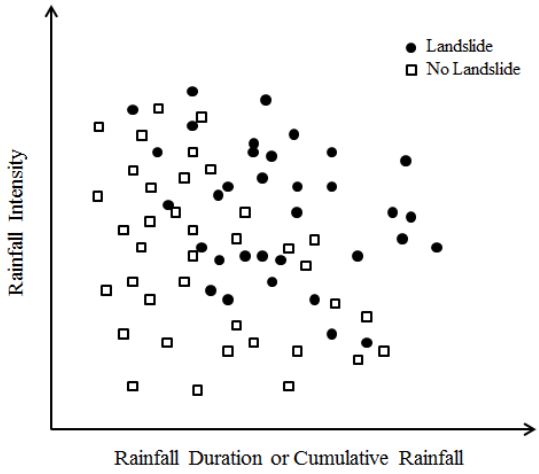

Fig. 1. Illustration of rainfall intensity-duration or intensity-cumulative rainfall thresholds in real cases (retraced following Berti et al., 2012).

where R is the accumulated rainfall (mm), I is the rainfall intensity (mm/hr), a is the gradient of line in R-I graph of landslide events, and $C_{max(min)}$ is maximum (minimum) constraint of value of C. The probabilistic rainfall thresholds have an advantage over the determinant thresholds in terms of the consideration of uncertainties. However, it still has the fundamental limitation that only rainfall is taken into account for landslide prediction.

Statistical approaches

The empirical approach has been successfully applied in landslide early warning systems, but it has limitations for the prediction of the spatial distribution of landslide occurrence. The statistical approach can be a good alternative to overcome this limitation. The main advantage of this method is that it considers several geo-environmental factors. Based on spatial distribution and analysis of those factors, the landslide risk map can be produced. Pardeshi et al. (2013) categorized the statistical methods into two groups as bi-variate statistical methods and multi-variate statistical methods.

The bi-variate statistical method compares data layers of geo-environmental factors to the observed landslide distribution data, and the weight is estimated by the landslide density. There are several bi-variate statistical methods: weights of evidence method, weighted overlay method, frequency ratio method, information value method, and fuzzy logic method.

The weight of evidence technique is based on the Bayesian probability approach. It uses different combinations of geophysical factors to find their interrelation. This method has been successfully applied in many reteaches (Ghosh et al., 2009; Blahut et al., 2010; Neuhäuser et al., 2011; Piacentini et al., 2012; Schicker and Moon, 2012; Martha et al., 2013). In the weighted overlay method, the weight is estimated based on the relationship of geophysical factors with the landslide frequency (Sarkar et al., 1995; Cardinali et al., 2002; Parise, 2002; Preuth et al., 2010). The frequency ratio method assesses the landslide susceptibility index by summing of the frequency ratios of each geophysical factor. The frequency ratio for each individual factor is estimated from the relationship between the factors and the landslide occurrence (Lee, 2005; Bălteanu et al., 2010; Goswami et al., 2011). In the information value method, the information values are determined for each subclass of landslide-related parameter on the basis of the presence of landslides in a

given mapping unit. This approach has proved to be a useful tool for determining the degree of influence of individual causative geophysical factor (Zêzere, 2002; Arora et al., 2004; Wang and Sassa, 2005; Champatiray et al., 2006). The fuzzy logic method defines explanatory variables between 0 and 1 based on the fuzzy theory. These variables are integrated using a fuzzy gama operator or a fuzzy algebraic sum to generate the spatial distribution map of the landslide.

As stated above bi-variate statistical methods consider individual geo-physical factor to the observed landslide occurrences, which may lead to a limitation of the method because the interrelation which exists among the landslide-causing factors and the landslide is basically the result of several causing factors. Therefore, approaches considering several factors at a time have been proposed for more accurate predictions of landslides. These methods are called multivariate statistical methods. The multivariate approach has widely been used since the past decade and proved to be a more objective method for assessing landslide hazards with complex geophysical data (Ercanoglu et al., 2004; Conoscenti et al., 2008; Van Den Eeckhaut et al., 2009). These methods compute the percentage of landslide area for each pixel based on multivariate analysis such as logistic regression, discriminant analysis, multiple regression, conditional analysis, and artificial neural network methods (Pardeshi et al., 2013).

The logistic regression predicts the presence or absence of a characteristic or outcome based on values of predictor variables. This model is useful for dichotomous events such as landslides. The logistic regression method finds the best fitting relationship between presence (or absence) of landslides and a set of geophysical factors such as slope angle, slope aspect, and land use (Ayalew and Yamagishi, 2005). Recently, this method has been applied in many reteaches (Ohlmacher and Davis, 2003; Chau et al., 2004; Ayalew et al., 2005; Ayalew and Yamagishi, 2005; Wang and Sassa, 2005; Chang et al., 2007; García-Rodríguez et al., 2008; Nefeslioglu et al., 2008; Ghosh et al., 2009; Erener and Düzgün, 2010; Akgun, 2011; Das et al., 2011).

The discriminant analysis method is one of the frequently used statistical methods for producing landslide hazard maps. The maximum difference for the landslide-causing factors between landslide group and non-landslide group can be found and weights for these factors are estimated by the discriminant analysis (Lee et al., 2008). This method has been successfully applied in several studies (Ohlmacher and Davis, 2003; Lee et al., 2008; Van Den Eeckhaut et al., 2009).

The artificial neural network method has also been applied for the prediction of landslide occurrence, which is triggered by complexly interrelated many factors. The complex correlations among many landslide-causing factors are expressed by the neurons and the layers (Catani et al., 2005; Ercanoglu, 2005; Pradhan and Lee, 2009; Tien Bui et al., 2012). Clerici et al. (2002) applied conditional analysis method for landslide prediction in GRASS (Geographical Research Analysis Support System), which is widely used open source GIS software.

Physical approaches

The empirical rainfall threshold can be used to predict the timing of landslide occurrence while the statistical approach can predict the spatial distribution of landslide susceptibility. Both methods have advantages and limitations as previously stated. On the other hand, the physically based models have the ability to predict both the spatial distribution of landslide susceptibility and the timing of landslide occurrence. They describe the physical triggering processes of shallow landslides and provide spatially variable slope - stability information, often as a safety factor (FS), which is an index expressing the ratio between the local resisting and driving force.

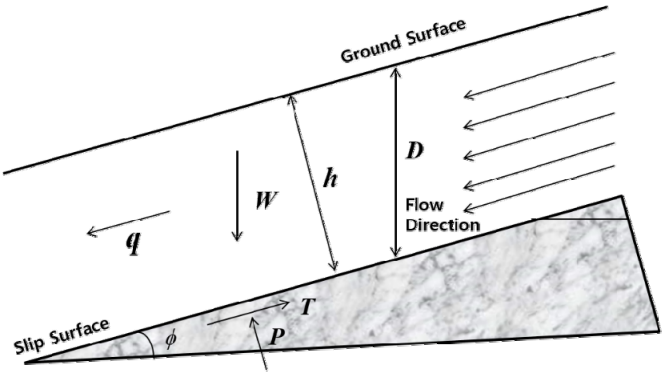

Fig. 2. Schematic of the infinite slope-stability model (An et al., 2016).

Most of the physically based model estimate FS based on the infinite slope stability model. Fig. 2 shows a schematic of an infinite slope - stability model. With assumption of an infinite slope and failure parallel to the slope surface the shear and normal stress are derived as follows:

$$\tau = \frac{T}{b/\cos\phi} = \frac{W}{b}\cos\phi\sin\phi \tag{3}$$

$$\sigma = \frac{P}{b/\cos\phi} = \frac{W}{b}\cos^2\phi \tag{4}$$

where $W = \gamma_s Db$ is the soil weight (kg/m), T is the shear force (kg/m), P is the normal force (kg/m), D is the soil depth (m), b is the slope width (m), ϕ is the slope angle (rad), and γ_s is the unit weight of the soil (kg/m^3). According to the Mohr - Coulomb theory, the shear strength of an infinite slope is as follows:

$$S = c + \sigma' \tan\varphi \tag{5}$$

where c is the cohesion (kg/m^2), σ' is the effective stress (kg/m^2), which was expressed as $\sigma' = \sigma - u$, u is the pore water pressure (kg/m^2), and φ is the angle of internal friction (rad). Then, the FS is defined as

$$FS = \frac{S}{\tau} \tag{6}$$

Substituting Eqs. (3) - (5) into Eq. (6) yields the following equation:

$$FS = \frac{c + \left(\gamma_s D\cos^2\phi - u\right)\tan\varphi}{\gamma_s D\sin\phi\cos\phi} \tag{7}$$

Substituting $u = \gamma_w \psi$ into Eq. (7) gives

$$FS = \frac{c + \left[D\gamma_s \cos^2 \phi - \gamma_w \psi \right] \tan \varphi}{\gamma_s D \sin \phi \cos \phi} \quad (8)$$

where γ_w is the unit weight of water (kg/m^3), and ψ is the pressure head of the subsurface water (m). Eq. (8) is rewritten by separating the time-variant term and steady terms as (Iverson, 2000)

$$FS = -\frac{\psi \gamma_w \tan \varphi}{\gamma_s D \sin \phi \cos \phi} + \frac{\tan \varphi}{\tan \phi} + \frac{c}{\gamma_s D \sin \phi \cos \phi} \quad (9)$$

Note that time-variant variable in Eq. (9) is only the pressure head and the other variables are steady in time. The pressure head can be estimated for steady and unsteady state.

Several studies (Montgomery and Dietrich, 1994; Pack et al., 1999) consider a simple steady-state hydrological process under constant rainfall to estimate the pressure head. They used the topographic wetness index, which is commonly used to quantify topographic control on hydrological processes. This index is a function of both the slope and the upstream contributing area per unit width orthogonal to the flow direction. The index can be converted to the pressure head with the assumption that the water is accumulated at the bottom of the slope. Therefore, the accuracy of the models is highly related to the estimation of the wetness index. Lee et al. (2012) compared the effects of several of the upstream contributing area estimation methods for wetness index. Many studies have applied steady-state approaches for the prediction of landslides (Acharya et al., 2005; Terhorst and Kreja, 2009; Gomes et al., 2013; Michel et al., 2014; Pradhan et al., 2014). The steady-state approaches are useful for producing spatially distributed slope stability but are limited to the temporal prediction of the slope stability because of the steady-state description of hydrological fluxes.

In order to estimate the unsteady pressure head in slope, the subsurface flow should be computed. The subsurface flow system of partially saturated soil is formulated by the Richards equation as follows

$$\frac{\partial \theta(\psi)}{\partial t} - \nabla \cdot \left(K(\psi) \nabla (\psi + z) \right) - q = 0 \quad (10)$$

where ψ is the pressure head (m); θ is the volumetric moisture content; K is the hydraulic conductivity (m/s); t is time (s); z is the vertical dimension, which is assumed to be positive in the upward direction; and q is the general source term (1/s), including rainfall.

Simoni et al., (2008) solved the three-dimensional (3D) subsurface flow numerically on the basis of Eq. (10) and considers the physical hydrological process for the estimation of landslide susceptibility. The computation of 3D subsurface flow usually requires a large amount of computational resources because fully implicit temporal discretization is essential for the numerical stability owing to the high nonlinearity of the Richards equation.

On the other hand, (Iverson, 2000; Baum et al., 2008) computed the transient pore-water pressure based on the one-dimensional (1D) Richards equation as follows:

$$\frac{\partial\theta(\psi)}{\partial t}-\frac{\partial}{\partial z}\left(K(\psi)\frac{\partial(\psi+z)}{\partial z}\right)+q=0 \tag{11}$$

Note that the above equation is not able to consider the effect of horizontal subsurface flow in slope. With the assumption of a simple exponential soil-water retention relationship, the analytical solution can be used, which can reduce the computational cost significantly. This model has been widely used in the past decade (Liu and Wu, 2007; Baum et al., 2010; Liao et al., 2010; Montrasio et al., 2011; Saadatkhah et al., 2014; Peres and Cancelliere, 2016), and its parallelized version has been developed (Alvioli and Baum, 2016).

Lu and Likos (2006) insist that Eq. (9) is only valid for saturated soil and Terzaghi's effective stress is unsatisfactory for unsaturated soil. If the soil is highly dried, the large negative pressure head causes an excessive suction force with a Terzaghi's effective stress of $\sigma' = \sigma - u$. They generalized the effective stress as follows:

$$\sigma' = \sigma - u_a + \sigma^s \tag{12}$$

where u_a is the air pressure, and σ^s is the suction stress, which is a characteristic function of the saturation or matric suction and is expressed in a closed form as follows:

$$\sigma^s = -(u_a - u_w)S_e \tag{13}$$

Here, u_w is the water pressure, and S_e is the effective saturation, which is defined as

$$S_e = \frac{\theta - \theta_r}{\theta_s - \theta_r} \tag{14}$$

where θ_s is the saturated moisture content, and θ_r is the residual moisture content. The assumption of $u_a = 0$ and $u_w = \psi\gamma_w$ leads an effective stress of $\sigma' = \sigma - \psi S_e\gamma_w$. Therefore, Eq. (9) is generalized for variably saturated soil as

$$FS = -\frac{\psi S_e\gamma_w \tan\varphi}{\gamma_s D\sin\phi\cos\phi} + \frac{\tan\varphi}{\tan\phi} + \frac{c}{\gamma_s D\sin\phi\cos\phi}. \tag{15}$$

Note that if the soil is saturated, the effective saturation becomes zero, and Eq. (15) is equivalent to Eq. (9).

An et al. (2016) proposed the landslide prediction model based on Eqs. (10) and (15). They also proposed the numerical scheme to reduce the computational requirement. They found that the proposed scheme significantly reduced the computation cost required for 3D physical modelling approaches.

Conclusion

For last two decades, landslide prediction techniques have achieved a significant progress with the remarkable

advance of the computer, GIS, and remote sensing technology. However, there are still many unknowns and uncertainties on the triggering process of the landslide because the landslide is a fundamentally complex hazard, which is related to hydrology, soil physics, meteorology, etc., and shows very different behaviors depending on the region. Several prediction methods are surveyed, and many previous studies are introduced in this article. There is no perfect methodology for landslide prediction to be applied everywhere since all of the prediction methods have limitations and strengths. Therefore, it is recommended that users or researchers consider the purpose of the prediction, the available data, human resources, social issues, and research period when selecting a landslide prediction method.

Acknowledgements

This work was supported by a research fund of Chungnam National University.

References

Acharya G, Smedt FD, Long NT. 2005. Assessing landslide hazard in GIS: A case study from Rasuwa, Nepal. Bull. Bulletin of Engineering Geology and the Environment 65:99-107.

Akgun A. 2011. A comparison of landslide susceptibility maps produced by logistic regression, multi-criteria decision, and likelihood ratio methods: A case study at İzmir, Turkey. Landslides 9: 93-106.

Aleotti P. 2004. A warning system for rainfall-induced shallow failures. Engineering Geology Rainfall-triggered landslides and debris flows 73:247-265.

Alvioli M, Baum RL. 2016. Parallelization of the TRIGRS model for rainfall-induced landslides using the message passing interface Environmental Modelling & Software 81:122-135.

An H, Viet TT, Lee G, Kim Y, Kim M, Noh S, Noh J. 2016. Development of time-variant landslide-prediction software considering three-dimensional subsurface unsaturated flow. Environmental Modelling & Software 85:172-183.

Arora MK, Gupta ASD, Gupta RP. 2004. An artificial neural network approach for landslide hazard zonation in the Bhagirathi (Ganga) Valley, Himalayas. International Journal of Remote Sensing 25:559-572.

Ayalew L, Yamagishi H, Marui H, Kanno T. 2005. Landslides in Sado Island of Japan: Part II. GIS-based susceptibility mapping with comparisons of results from two methods and verifications. Engineering Geology 81:432–445.

Ayalew L, Yamagishi H. 2005. The application of GIS-based logistic regression for landslide susceptibility mapping in the Kakuda-Yahiko Mountains. Central Japan. Geomorphology 65:15-31.

Bălteanu D, Chendeş V, Sima M, Enciu P. 2010. A country-wide spatial assessment of landslide susceptibility in Romania. Geomorphology, Recent advances in landslide investigation 124:102-112.

Baum RL, Godt JW, Savage WZ. 2010. Estimating the timing and location of shallow rainfall-induced landslides using a model for transient, unsaturated infiltration. Journal of Geophysical Research: Earth Surface 115:F03013.

Baum RL, Godt JW. 2009. Early warning of rainfall-induced shallow landslides and debris flows in the USA. Landslides 7:259-272.

Baum RL, Savage WZ, Godt JW. 2008. TRIGRS-A fortran program for transient rainfall infiltration and grid-based regional slope-stability analysis, version 2.0. Geological Survey Open-File Report.

Berti M, Martina MLV, Franceschini S, Pignone, S, Simoni A, Pizziolo M. 2012. Probabilistic rainfall thresholds for landslide occurrence using a Bayesian approach. Journal of Geophysical Research: Earth Surface 117:F04006.

Blahut J, van Westen CJ, Sterlacchini S. 2010. Analysis of landslide inventories for accurate prediction of debris-flow source areas. Geomorphology 119:36–51.

Caine N. 1980. The rainfall intensity: Duration control of shallow landslides and debris flows. Geografiska Annaler. Series A, Physical Geography 62:23-27.

Campbell RH. 1975. Soil slips, debris flows, and rainstorms in the Santa Monica mountains and vicinity, Southern California. U.S. Govt. Print. Off.

Cannon SH, Gartner JE, Wilson RC, Bowers JC, Laber JL. 2008. Storm rainfall conditions for floods and debris flows from recently burned areas in southwestern Colorado and Southern California. Geomorphology 96:20.

Cardinali M, Reichenbach P, Guzzetti F, Ardizzone F, Antonini G, Galli M, Cacciano M, Castellani M, Salvati P. 2002. A geomorphological approach to the estimation of landslide hazards and risks in Umbria, Central Italy. Natural Hazards and Earth System Science 2:57-72.

Carrara A, Cardinali M, Guzzetti F, Reichenbach P. 1995. GIS technology in mapping landslide hazard. In *Geographical information systems in assessing natural hazards, Advances in natural and technological hazards research* edited by Carrara A, Guzzetti F. pp. 135–175. Springer, Netherlands.

Catani F, Casagli N, Ermini L, Righini G, Menduni G. 2005. Landslide hazard and risk mapping at catchment scale in the Arno River basin. Landslides 2:329-342.

Champatiray PK, Dimri S, Lakhera RC, Sati S. 2006. Fuzzy-based method for landslide hazard assessment in active seismic zone of Himalaya. Landslides 4:101.

Chang KT, Chiang SH, Hsu ML. 2007. Modeling typhoon-and earthquake-induced landslides in a mountainous watershed using logistic regression. Geomorphology 89:335–347.

Chau KT, Sze YL, Fung MK, Wong WY, Fong EL, Chan LCP. 2004. Landslide hazard analysis for Hong Kong using landslide inventory and GIS. Computers & Geosciences 30:429-443.

Clerici A, Perego S, Tellini C, Vescovi P. 2002. A procedure for landslide susceptibility zonation by the conditional analysis method. Geomorphology 48:349-364.

Conoscenti C, Di Maggio C, Rotigliano E. 2008. GIS analysis to assess landslide susceptibility in a fluvial basin of NW Sicily (Italy). Geomorphology, GIS technology and models for assessing landslide hazard and risk 94:325-339.

Das I, Stein A, Kerle N, Dadhwal VK. 2011. Probabilistic landslide hazard assessment using homogeneous susceptible units (HSU) along a national highway corridor in the northern Himalayas, India. Landslides 8:293-308.

Ercanoglu M, Gokceoglu C, Asch TWJV. 2004. Landslide Susceptibility zoning north of Yenice (NW Turkey) by multivariate statistical techniques. Natural Hazards 32:1-23.

Ercanoglu M. 2005. Landslide susceptibility assessment of SE Bartin (West black sea region, Turkey) by artificial neural networks. Natural Hazards Earth System Science 5:979-992.

Erener A, Düzgün HSB. 2010. Improvement of statistical landslide susceptibility mapping by using spatial and global regression methods in the case of More and Romsdal (Norway). Landslides 7:55-68.

García-Rodríguez MJ, Malpica JA, Benito B, Díaz M. 2008. Susceptibility assessment of earthquake-triggered landslides in El Salvador using logistic regression. Geomorphology 95:172-191.

Ghosh S, Westen CJ, Carranza EJM, Ghoshal TB, Sarkar NK, Surendranath M. 2009. A quantitative approach for improving the BIS (Indian) method of medium-scale landslide susceptibility. Journal of the Geological Society of India 74:625.

Glade T, Crozier M, Smith P. 2000. Applying probability determination to refine landslide-triggering rainfall thresholds using an empirical “Antecedent daily rainfall model.” Pure and Applied Geophysics 157:1059-1079.

Gomes RAT, Guimarães RF, de Carvalho J, Fernandes NF, do Amaral Júnior EV. 2013. Combining spatial models for shallow landslides and debris-flows prediction. Remote Sensing 5:2219-2237.

Goswami R, Mitchell NC, Brocklehurst SH. 2011. Distribution and causes of landslides in the eastern Peloritani of NE Sicily and western Aspromonte of SW Calabria, Italy. Geomorphology 132:111-122.

Greco R, Giorgio M, Capparelli G, Versace P. 2013. Early warning of rainfall-induced landslides based on empirical mobility function predictor. Engineering Geology 153:68-79.

Guidicini G, Iwasa OY. 1997. Tentative correlation between rainfall and landslides in a humid tropical environment. Bulletin of the International Association of Engineering Geology 16:13-20.

Guo X, Cui P, Li Y, 2013. Debris flow warning threshold based on antecedent rainfall: A case study in Jiangjia Ravine, Yunnan, China. Journal of Mountain Science 10:305-314.

Guzzetti F, Peruccacci S, Rossi M, Stark CP. 2007a. The rainfall intensity-duration control of shallow landslides and debris flows: An update. Landslides 5:3-17.

Guzzetti F, Peruccacci S, Rossi M, Stark CP. 2007b. Rainfall thresholds for the initiation of landslides in Central and Southern Europe. Meteorology and Atmospheric Physics 98:239-267.

Hong Y, Hiura H, Shino K, Sassa K, Suemine A, Fukuoka H, Wang G. 2005. The influence of intense rainfall on the activity of large-scale crystalline schist landslides in Shikoku Island, Japan. Landslides 2:97-105.

Huabin W, Gangjun L, Weiya X, Gonghui W. 2005. GIS-based landslide hazard assessment: An overview. Progress in Physical Geography 29:548-567.

Huang J, Ju NP, Liao YJ, Liu DD. 2015. Determination of rainfall thresholds for shallow landslides by a probabilistic and empirical method. Natural Hazards Earth System Science 15: 2715-2723.

Iverson RM. 1997. The physics of debris flows. Reviews of Geophysics 35:245-296.

Iverson RM. 2000. Landslide triggering by rain infiltration. Water Resources Research 36:1897-1910.

Keefer DK, Wilson RC, Mark RK, Brabb EE, Brown WM, Ellen SD, Harp EL, Wieczorek GF, Alger CS, Zatkin RS. 1987. Real-time landslide warning during heavy rainfall. Science 238:921-925.

Kim D, Lee EJ, Ahn B, Im S. 2014. Landslide Susceptibility mapping using a grid-based infiltration transient model in mountainous regions. In *Landslide science for a safer geoenvironment* edited by Sassa K, Canuti P, Yin Y. pp. 425-429. Springer International Publishing.

Lee CT, Huang CC, Lee JF, Pan KL, Lin ML, Dong JJ. 2008. Statistical approach to storm event-induced landslides susceptibility. Natural Hazards Earth System Science 8:941-960.

Lee G, Oh S, An H, Jung K. 2012. A comparative analysis on slope stability using specific catchment area calculation. Journal of Korea Water Resources Association 45:643-656.

Lee JH, Park HJ. 2014. GIS-based probabilistic analysis of shallow landslide susceptibility using a transient hydrogeological model and Monte Carlo simulation. In *Landslide science for a safer geoenvironment* edited by Sassa K, Canuti P, Yin Y. pp. 451-456. Springer International Publishing.

Lee S. 2005. Application of logistic regression model and its validation for landslide susceptibility mapping using GIS and remote sensing data. International Journal of Remote Sensing 26: 1477-1491.

Liao Z, Hong Y, Kirschbaum D, Adler RF, Gourley JJ, Wooten R. 2010. Evaluation of TRIGRS (transient rainfall infiltration and grid-based regional slope-stability analysis)'s predictive skill for hurricane-triggered landslides: A case study in Macon County, North Carolina. Natural Hazards 58:325-339. doi:10.1007/s11069-010-9670-y

Liu CN, Wu CC. 2007. Mapping susceptibility of rainfall-triggered shallow landslides using a probabilistic approach. Environmental Geology 55:907-915.

Lu N, Likos WJ. 2006. Suction stress characteristic curve for unsaturated soil. Journal of Geotechnical and Geoenvironmental

Engineering 132:131-142.

Lumb P. 1975. Slope failures in Hong Kong. Quarterly Journal of Engineering Geology and Hydrogeology 8:31-65.

Martha TR, van Westen CJ, Kerle N, Jetten V, Vinod Kumar K. 2013. Landslide hazard and risk assessment using semi-automatically created landslide inventories. Geomorphology 184:139-150.

Michel GP, Kobiyama M, Goerl RF. 2014. Comparative analysis of SHALSTAB and SINMAP for landslide susceptibility mapping in the Cunha River basin, Southern Brazil. Journal of Soils and Sediments 14:1266-1277.

Montgomery DR, Dietrich WE. 1994. A physically based model for the topographic control on shallow landsliding. Water Resources Research 30:1153-1171.

Montrasio L, Valentino R, Losi GL. 2011. Towards a real-time susceptibility assessment of rainfall-induced shallow landslides on a regional scale. Natural Hazards Earth System Science 11:1927-1947.

Nefeslioglu AT, Duman TY, Durmaz S. 2008. Landslide susceptibility mapping for a part of tectonic Kelkit Valley (Eastern Black Sea region of Turkey). Geomorphology, GIS technology and models for assessing landslide hazard and risk 94:401-418.

Neuhäuser B, Damm B, Terhorst B. 2011. GIS-based assessment of landslide susceptibility on the base of the Weights-of-Evidence model. Landslides 9:511-528.

Ohlmacher GC, Davis JC. 2003. Using multiple logistic regression and GIS technology to predict landslide hazard in northeast Kansas, USA. Engineering Geology 69:331-343.

Osanai N, Shimizu T, Kuramoto K, Kojima S, Noro T. 2010. Japanese early-warning for debris flows and slope failures using rainfall indices with Radial Basis Function Network. Landslides 7:325-338.

Pack RT, Tarboton DG, Goodwin CN. 1999. SINMAP 2.0 - A stability index approach to terrain stability hazard mapping, User's Manual.

Pardeshi SD, Autade SE, Pardeshi SS. 2013. Landslide hazard assessment: Recent trends and techniques. SpringerPlus 2:523.

Parise M. 2002. Landslide hazard zonation of slopes susceptible to rock falls and topples. Natural Hazards Earth System Science 2:37-49.

Peres DJ, Cancelliere A. 2016. Estimating return period of landslide triggering by Monte Carlo simulation. Journal of Hydrology 541:256-271.

Piacentini D, Troiani F, Soldati M, Notarnicola C, Savelli D, Schneiderbauer S, Strada C. 2012. Statistical analysis for assessing shallow-landslide susceptibility in South Tyrol (south-eastern Alps, Italy). Geomorphology 151-152:196-206.

Pradhan AMS, Oh JR, Jung MS, Kim YT. 2014. Predictive capability of deterministic and statistical models in weathered granite soil watershed, In Landslide science for a safer geoenvironment edited by Sassa K, Canuti P, Yin Y. pp. 507–512. Springer International Publishing.

Pradhan B, Lee S. 2009. Regional landslide susceptibility analysis using back-propagation neural network model at Cameron Highland, Malaysia. Landslides 7:13-30.

Preuth T, Glade T, Demoulin A. 2010. Stability analysis of a human-influenced landslide in eastern Belgium. Geomorphology, Landslide geomorphology in a changing environment 120:38-47.

Saadatkhah N, Kassim A, Lee LM. 2014. Hulu Kelang, Malaysia regional mapping of rainfall-induced landslides using TRIGRS model. Arabian Journal of Geosciences 8:3183-3194.

Sarkar S, Kanungo DP, Mehrotra GS. 1995. Landslide hazard zonation: A case study in Garhwal Himalaya, India. Mountain Research and Development 15:301-309.

Schicker R, Moon V. 2012. Comparison of bivariate and multivariate statistical approaches in landslide susceptibility mapping at a regional scale. Geomorphology 161-162:40-57.

Segoni S, Battistini A, Rossi G, Rosi A, Lagomarsino D, Catani F, Moretti S. Casagli, N. 2015. Technical note: An operational landslide early warning system at regional scale based on space-time-variable rainfall thresholds. Natural Hazards Earth System Science 15:853-861.

Segoni S, Rosi A, Rossi G, Catani F, Casagli N. 2014. Analysing the relationship between rainfalls and landslides to define a mosaic of triggering thresholds for regional-scale warning systems. Natural Hazards Earth System Science 14:2637-2648.

Simoni S, Zanotti F, Bertoldi G, Rigon R. 2008. Modelling the probability of occurrence of shallow landslides and channelized debris flows using GEOtop-FS. Hydrological Processess 22:532-545.

Terhorst B, Kreja R. 2009. Slope stability modelling with SINMAP in a settlement area of the Swabian Alb. Landslides 6:309-319.

Tien Bui D, Pradhan B, Lofman O, Revhaug I, Dick OB. 2012. Landslide susceptibility assessment in the Hoa Binh province of Vietnam: A comparison of the Levenberg-Marquardt and Bayesian regularized neural networks. Geomorphology:171-172, 12-29.

Van Den Eeckhaut M, Reichenbach P, Guzzetti F, Rossi M, Poesen J. 2009. Combined landslide inventory and susceptibility assessment based on different mapping units: An example from the Flemish Ardennes, Belgium. Natural Hazards Earth System Science 9:507-521.

Wang HB, Sassa K. 2005. Comparative evaluation of landslide susceptibility in Minamata area, Japan. Environmental Geology 47:956-966.

Westen CJ, van Rengers N, Terlien MTJ, Soeters R. 1997. Prediction of the occurrence of slope instability phenomenal through GIS-based hazard zonation. Geologische Rundschau 86:404-414.

Zêzere JL, Vaz T, Pereira S, Oliveira SC, Marques R, Garcia RAC. 2014. Rainfall thresholds for landslide activity in Portugal: A state of the art. Environmental Earth Sciences 73:2917-2936.

Zêzere JL. 2002. Landslide susceptibility assessment considering landslide typology. A case study in the area north of Lisbon (Portugal). Natural Hazards and Earth System Sciences 2:73-82.